Acta Mech Sin (2007) 23:43–48
DOI 10.1007/s10409-006-0053-2

RESEARCH PAPER

Bifurcation of thermocapillary convection in a shallow annular pool of silicon melt

Yourong Li · Lan Peng · Shuangying Wu · Nobuyuki Imaishi

Received: 26 September 2005 / Revised: 18 August 2006 / Accepted: 4 September 2006 / Published online: 6 January 2007

Abstract In order to understand the nature of surface patterns on silicon melts in industrial Czochralski furnaces, we conducted a series of unsteady three-dimensional numerical simulations of thermocapillary convections in thin silicon melt pools in an annular container. The pool is heated from the outer cylindrical wall and cooled at the inner wall. Bottom and top surfaces are adiabatic. The results show that the flow is steady and axisymmetric at small temperature difference in the radial direction. When the temperature difference exceeds a certain threshold value, hydrothermal waves appear and bifurcation occurs. In this case, the flow is unsteady and there are two possible groups of hydrothermal waves with different number of waves, which are characterized by spoke patterns traveling in the clockwise and counter-clockwise directions. Details of the flow and temperature disturbances are discussed and number of waves and traveling velocity of the hydrothermal wave are determined.

Keywords Computer simulation · Thermocapillary convection · Semiconducting silicon · Bifurcation

The project supported by the National Natural Science Foundation of China (50476042) and the Scientific Research Foundation for the Returned Overseas Chinese Scholars, Ministry of Education of China. The English text was polished by Yunming Chen.

Y. Li (✉) · L. Peng · S. Wu
College of Power Engineering, Chongqing University, Chongqing 400044, China
e-mail: liyourong@cqu.edu.cn

N. Imaishi
Institute for Materials Chemistry and Engineering, Kyushu University, Fukuoka 816-8580, Japan

1 Introduction

In the past few decades, thermocapillary convection has received much attention with respect to both fundamental and industrial aspects, especially in microgravity-related fluid science and in semiconductor single-crystal growth from melt. In the terrestrial environment, buoyancy and thermocapillary forces are coupled to cause natural convections. However, under microgravity or in shallow fluid layers on the earth, the thermocapillary force becomes dominant. Smith and Davis [1] performed a linear stability analysis of a thin and infinitely extended fluid layer with a free upper surface subjected to a constant horizontal temperature gradient. They found two types of three-dimensional (3-D) instabilities, i.e. stationary longitudinal rolls and oblique hydrothermal waves depending on the Prandtl number (Pr) and the basic flow pattern (with or without a return flow), determined the critical Marangoni number. Subsequently, Garnier and Normand [2] performed a linear stability analysis of radial thermocapillary flow in an extended cylindrical geometry for liquids with $Pr = 10$ and predicted that the instability appeared first near the inner cylinder.

Many experiments of thermocapillary convection in a shallow liquid layer subjected to a horizontal temperature gradient were performed for rectangular geometries [3–12], annular geometry [13–16] and Czochralski configuration [17,18] with cold liquids. In these experiments, high-Pr fluids, such as silicone oils, molten salts and acetone, were used, and authors of these experiments reported various types of flow instabilities. However, few experimental reports are known on thermocapillary convection in low-Pr fluids, such as liquid metals. Recently, Azami et al. [19] observed spoke patterns on the surface of a shallow, annular pool of high-temperature silicon melt (3 and 8 mm in depth) and reported that thermocapillary flow might play an important role in the incipience of 3-D convection and the number of spokes.

Numerical simulations have facilitated the understanding of the characteristics of thermocapillary convection. Ben Hadid and Roux [20,21] performed two-dimensional (2-D) simulations of thermocapillary-buoyancy and pure thermocapillary convection in pools of low-*Pr* fluids with various aspect ratios in rectangular geometries, and shown the existence of a multicellular steady flow and a transition to oscillatory convection. Villers and Platten [3] carried out both experiments and 2-D simulations for acetone ($Pr = 4$), and confirmed the existence of a multicellular flow. Li et al. [22], Xu and Zebib [23] performed 2-D and 3-D calculations for fluids with moderate *Pr* number. They determined the Hopf bifurcation neutral curves as a function of capillary Reynolds number and aspect ratio. Recently, we performed series of numerical simulations of 3-D thermocapillary-buoyancy flows with different *Pr* numbers in different geometric configurations [24–26] and suggested that thermocapillary flow subjected to a radial temperature gradient would exhibit several types of 3-D oscillations. These flow types depend on the *Pr* number, liquid depth, buoyancy, geometry and temperature gradients. In this paper, we present a series of unsteady 3-D numerical simulations to understand the bifurcation characteristics of thermocapillary convections of silicon melt in shallow annular layers subjected to a radial temperature gradient.

2 Model formulation

2.1 Basic assumptions and governing equations

We analyze the flow of silicon melt in a shallow annular layer of depth $d = 3$ mm, inner radius $r_i = 15$ mm and outer radius $r_o = 50$ mm, with a free upper surface and a solid bottom, as shown in Fig. 1. The inner and outer cylinders are maintained at constant temperatures T_c and T_h, ($T_h > T_c = T_m$), respectively. The horizontal temperature gradient varies in the radial direction. The thermocapillary force is taken into account at the top free surface, whereas at other solid–liquid boundaries no-slip condition is applied. Melt convection is generated by the surface tension gradient on the top surface. The following assumptions are introduced in our model: (1) Silicon melt is an incompressible Newtonian fluid and the properties are constant except for the surface tension; (2) The velocity is small and the flow is laminar; (3) The upper surface is flat and nondeformable.

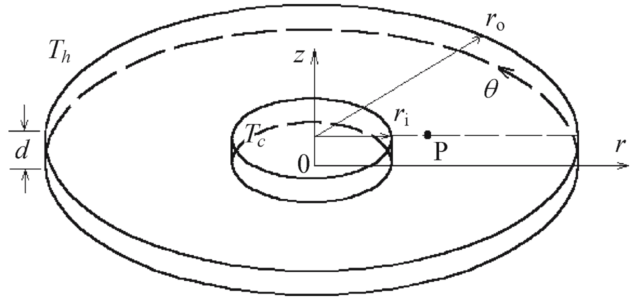

Fig. 1 Configuration of the system

With the above assumptions, the flow and heat transfer equations are expressed in a nondimensional form as follows:

$$\nabla \cdot \boldsymbol{V} = 0, \tag{1}$$

$$\frac{\partial \boldsymbol{V}}{\partial \tau} + \boldsymbol{V} \cdot \nabla \boldsymbol{V} = -\nabla P + \nabla^2 \boldsymbol{V} + Gr\Theta \boldsymbol{e}_Z, \tag{2}$$

$$\frac{\partial \Theta}{\partial \tau} + \boldsymbol{V} \cdot \nabla \Theta = \frac{1}{Pr}\nabla^2 \Theta. \tag{3}$$

The boundary conditions are: at the free surface ($Z = d/r_o$, $R_i < R < 1, 0 \le \theta < 2\pi$)

$$\frac{\partial V_R}{\partial Z} = -Re_\gamma \frac{\partial \Theta}{\partial R}, \tag{4a}$$

$$\frac{\partial V_\theta}{\partial Z} = -Re_\gamma \frac{\partial \Theta}{R\partial \theta}, \tag{4b}$$

$$V_Z = 0, \tag{4c}$$

$$\frac{\partial \Theta}{\partial Z} = 0, \tag{4d}$$

at the bottom ($Z = 0, R_i < R < 1, 0 \le \theta < 2\pi$)

$$V_R = V_\theta = V_Z = 0, \tag{5a–c}$$

$$\frac{\partial \Theta}{\partial Z} = 0, \tag{5d}$$

at the inner cylinder ($R = R_i$, $0 \le Z \le d/r_o$, $0 \le \theta < 2\pi$)

$$V_R = V_\theta = V_Z = 0, \tag{6a–c}$$

$$\Theta = \Theta_i = 0, \tag{6d}$$

and at the outer cylinder ($R = 1, 0 \le Z \le d/r_o, 0 \le \theta < 2\pi$)

$$V_R = V_\theta = V_Z = 0, \tag{7a–c}$$

$$\Theta = \Theta_o = 1. \tag{7d}$$

The initial conditions are expressed as follows (at $\tau = 0$):

$$V_R = V_\theta = V_Z = 0, \tag{8a–c}$$

$$\Theta = 1 - \ln R/ \ln R_i, \tag{8d}$$

where $\boldsymbol{V}$ is the velocity vector, P the pressure, Θ the temperature, τ the time in nondimensional form. R, Z and θ are the cylindrical coordinates. $\boldsymbol{e}_Z$ is the Z-directional unit vector. The nondimensional parameters $Gr = \frac{\rho_T g \Delta T r_{\mathrm{o}}^3}{\nu^2}$, $Pr = \frac{\nu}{a}$ and $Re_\gamma = \frac{\gamma_T \Delta T r_{\mathrm{o}}}{\mu\nu}$ are the Grashof number, the Prandtl number and the capillary Reynolds number, respectively, where $\Delta T = T_h - T_c$. ρ_T is the thermal expansion coefficient, ν the kinematic viscosity, a the thermal diffusivity, μ the viscosity and $\gamma_T = -\partial\gamma/\partial T$ the temperature coefficient of the surface tension.

The variables are nondimensionalized as

$$(R, Z) = \frac{(r, z)}{r_{\mathrm{o}}},$$
$$(V_R, V_\theta, V_Z) = \frac{(v_r, v_\theta, v_z)}{\nu/r_{\mathrm{o}}},$$
$$P = \frac{p r_{\mathrm{o}}^2}{\rho\nu^2},$$
$$\Theta = \frac{T - T_c}{T_h - T_c},$$
$$\tau = \frac{t\nu}{r_{\mathrm{o}}^2}.$$

The temperature difference in the radial direction is expressed in non-dimensionalized form as the Marangoni number [24],

$$Ma = \frac{\gamma_T d^2}{\mu\alpha}\frac{\Delta T}{r_{\mathrm{o}} - r_{\mathrm{i}}}.$$

The thermophysical properties of silicon melt at $T_m = 1683\,\mathrm{K}$ are listed below:

Thermal conductivity,	$\lambda = 64\,\mathrm{W\,m^{-1}\,K^{-1}}$,
Viscosity,	$\mu = 7.0 \times 10^{-4}\,\mathrm{kg\,m^{-1}\,s^{-1}}$,
Density,	$\rho = 2530\,\mathrm{kg\,m^{-3}}$,
Surface tension coefficient,	$\gamma_T = -7.0 \times 10^{-5}\,\mathrm{N\,m^{-1}\,K^{-1}}$,
Heat capacity,	$C_p = 1000\,\mathrm{J\,kg^{-1}\,K^{-1}}$,
Melting temperature,	$T_m = 1683\,\mathrm{K}$.

The temperature coefficient of the surface tension is assumed to be $-7 \times 10^{-5}\,\mathrm{N/(m\,K)}$ [27,28].

2.2 Numerical method

The fundamental equations are discretized by the finite-volume method. The modified central difference approximation is applied to the diffusion terms while the QUICK scheme is used for the convective terms. The SIMPLER algorithm [29] is used to handle the pressure–velocity coupling. In this study, nonuniform staggered grid of $60^r \times 30^z \times 60^\theta$ is used. The validation of the code and the grid convergence for the thermocapillary flow simulation were checked in Refs. [24–26].

Numerical simulations were conducted on an MPU of the Fujitsu VPP700 at the Computer Center of Kyushu University. The time increment was chosen between 10^{-4} and 10^{-3} s. The convergence at each time step was assumed if the maximum residual error of the continuity equation among all control volumes became less than $10^{-5}\,\mathrm{s^{-1}}$.

3 Results and discussion

Any radial temperature difference ($\Delta T = T_h - T_c > 0$) produces a surface tension gradient on the free surface of the melt and the Marangoni effect induces the flow in the melt layer. In the present case, surface fluid flows from the outer cylinder wall toward the inner cylinder wall and the recirculation flow exists near the bottom. If the Marangoni number Ma is small, the flow is steady and axisymmetric. This type of flow is called as the basic flow. However, when Ma is increased, this basic flow becomes unstable against 3-D disturbances. The critical condition for this flow transition is $Ma_{\mathrm{cri}} = 9.15 (\Delta T_{\mathrm{cri}} = 9\,\mathrm{K})$, as pointed out in Ref. [24].

When Ma exceeds a certain threshold value, 3-D disturbances are incubated and their amplitudes increase with time. Finally, a 3-D oscillatory flow pattern is formed. In order to get all possible solutions of the 3-D oscillatory flow and save the computation time, we use the V_R, V_Z and Θ values at $Ma = 8.13$ ($\Delta T = 8\,\mathrm{K}$) as the initial conditions and choose the time increment between 10^{-4} and 10^{-3} seconds when $Ma > Ma_{\mathrm{cri}}$. It is found that there are two groups of oscillatory flows and temperature fields with an azimuthal direction symmetry when Ma exceeds the critical value. Figure 2 shows

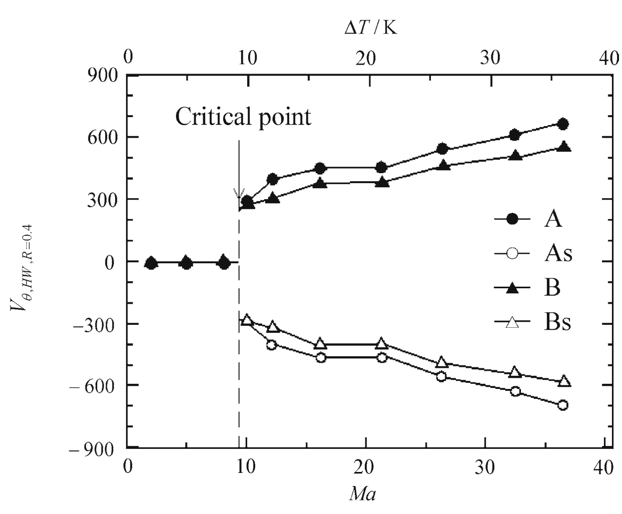

Fig. 2 Bifurcation diagram

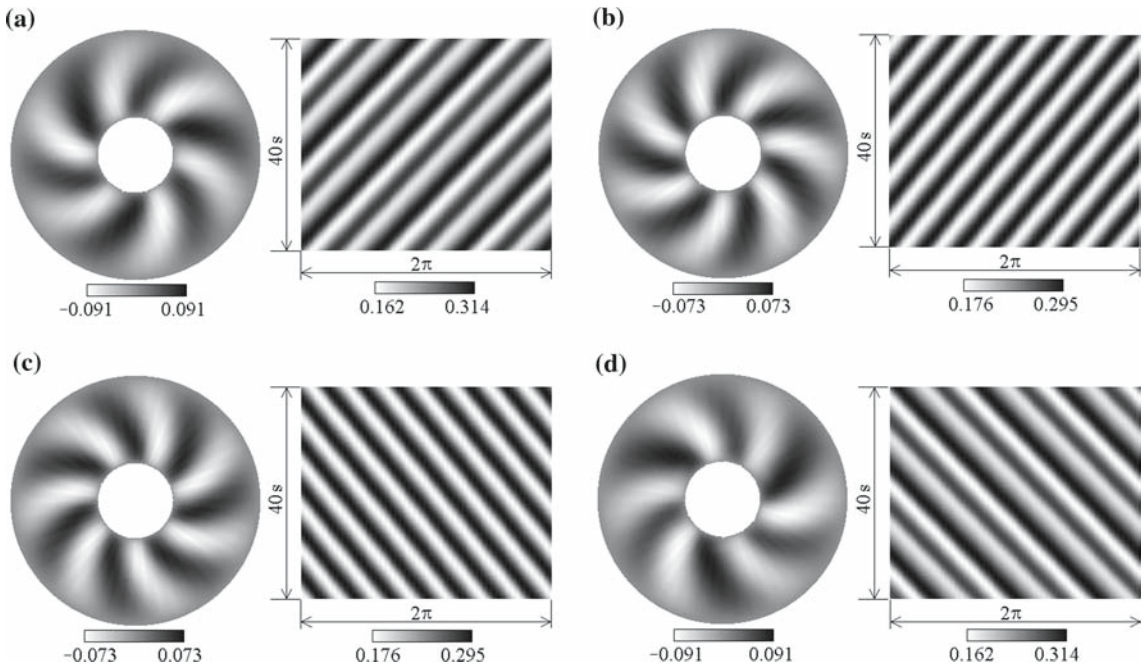

Fig. 3 Snapshots of surface temperature (left) and space-time diagram of surface temperature distribution (right) at $R = 0.4$ and $Ma = 21.35$ ($\Delta T = 21$ K). **a** A; **b** B; **c** Bs; **d** As

the propagating azimuthal velocity $V_{\theta,HW,R=0.4}$ of the oscillatory flow as a function of Ma at $R = 0.4$.

The temperature fluctuation $\delta\Theta$ is introduced to extract the 3-D disturbances:

$$\delta\Theta(R,\theta,Z,\tau) = \Theta(R,\theta,Z,\tau) - \frac{1}{2\pi}\int_0^{2\pi}\Theta(R,\theta,Z,\tau)\mathrm{d}\theta. \tag{10}$$

In this case, many traveling curved spoke patterns are observed on the entire surface. These correspond to the "hydrothermal wave" instability. For example, when $Ma = 21.35(\Delta T = 21\,\mathrm{K})$, as shown in Fig. 3, there are two possible traveling waves with the azimuthal direction symmetry. In Figs. 3a and d, six hot (dark) and six cold (bright) spots of comparable intensity indicate the mode (number of waves) $m = 6$. In this case, the hydrothermal waves are propagating in both the clockwise and counterclockwise directions with the numbers of spokes m=6. In Figs. 3b and c, the hydrothermal waves are also propagating in both the clockwise and counterclockwise directions but with $m = 7$. The angles (ϕ) between the wave propagation and the radial direction, measured at $R = 0.4$ ($r = 20$ mm), are about 75°–80° and 100°–105°, which is close to the angle values predicted by the linear stability theory for infinite rectangular layer [1]. However, as seen from Fig. 3, the spokes are not straight. Therefore, these traveling waves are taken as indication of many parallel tilted straight lines on the space-time diagram (STD) taken at $R = 0.4$.

The circumferential view of the temperature distribution and the flow structure at $R = 0.5$ ($r = 25$ mm) is shown in Fig. 4 for the case of $Ma = 21.35$ ($\Delta T = 21$ K). In this case, the annular pool was occupied by the hydrothermal waves propagating in the counterclockwise (Figs. 4a and b) and clockwise (Figs. 4c and d) directions. The hydrothermal waves are maintained by a coupling of temperature and velocity disturbances as described in Refs. [1,11].

Another way to recognize the type of waves established in the melt is to calculate a net azimuthal flow. The net azimuthal flow is determined as an integral,

$$V_{\theta,ave} = \frac{1}{\pi(1-R_{\mathrm{i}}^2)Z_d}\iiint V_\theta(R,\theta,Z,\tau)R\mathrm{d}Z\mathrm{d}R\mathrm{d}\theta. \tag{11}$$

The net azimuthal flow is shown in Fig. 5. It confirms that the flow pattern is 2-D flow ($V_{\theta,ave} = 0$) when Ma is small. After the bifurcation, the net azimuthal flow starts to grow. One azimuthal flow is along the counterclockwise direction and another along the clockwise one, which are accordant with the velocity of hydrothermal wave shown in Fig. 2. And the net azimuthal flow with small number of waves is faster than one with larger number of waves.

Figure 6 shows the amplitude and frequency of local surface temperature oscillations at a monitoring point P ($R = 0.4$, $\theta = 0$, $Z = 0.06$) and the number of waves as functions of Ma. Obviously, the amplitude increases with Ma while the frequency is less sensitive to Ma. These

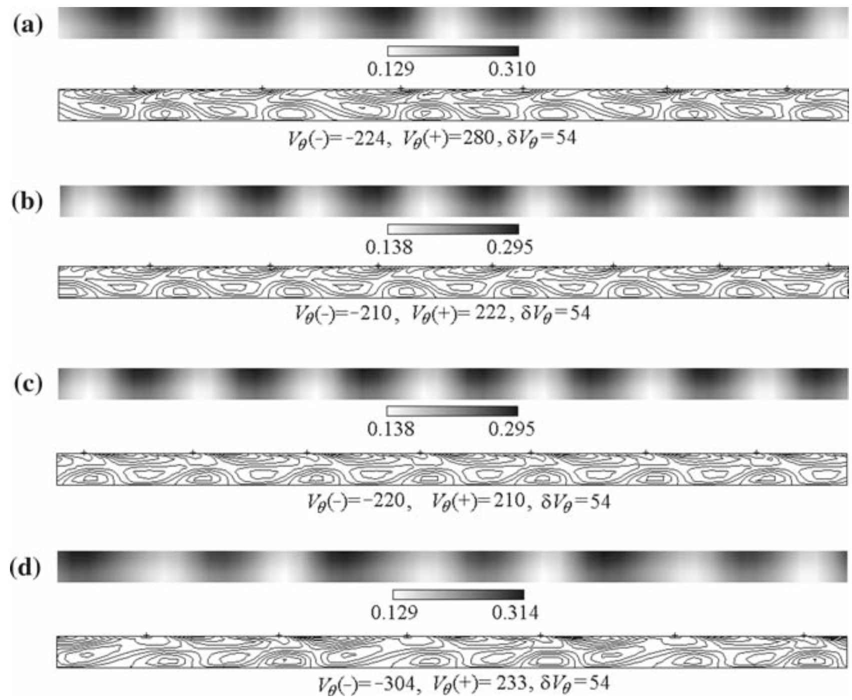

Fig. 4 The circumferential view of temperature distribution and flow structure at $\tau = 0.0166$ and $R = 0.5$ for $Ma = 21.35$ ($\Delta T = 21$ K). **a** A; **b** B; **c** Bs; **d** As

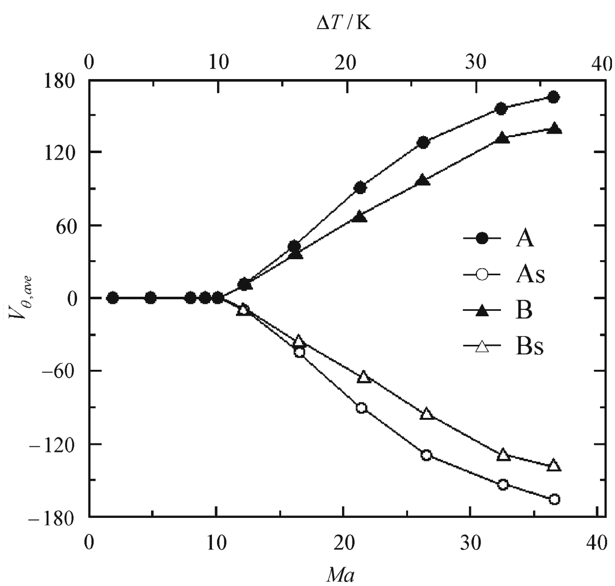

Fig. 5 Net azimuthal flow, defined by Eq. (11) vs. *Ma*

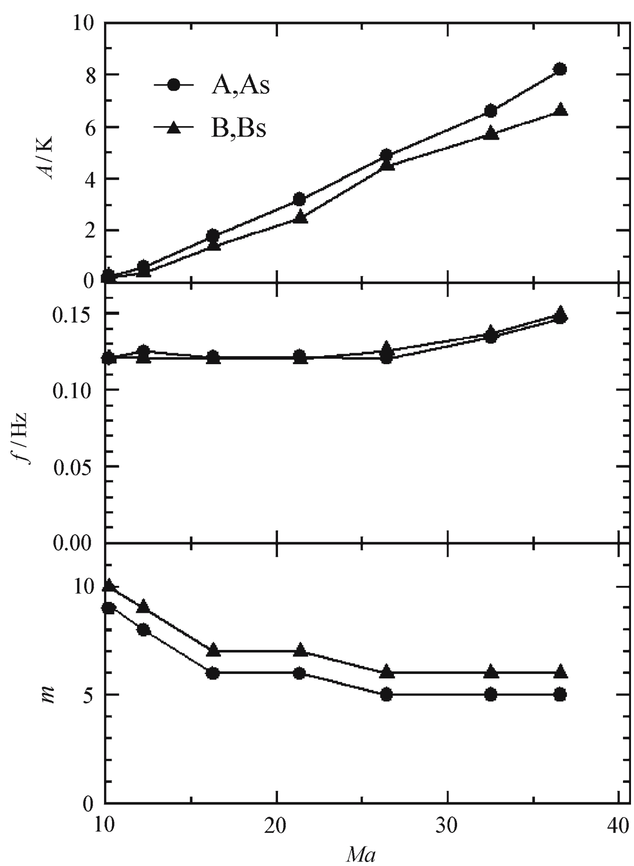

Fig. 6 Variation of amplitude A, frequency f and number of waves m at monitoring point P as functions of *Ma*

trends are similar to the experimental results for high-*Pr* fluids in the extended cylindrical vessel (cf. Fig. 3 of Ref. [15]) and the experimental results for high-*Pr* fluids in the rectangular shallow layer (cf. Fig. 10b of Ref. [11]).

4 Conclusions

A series of 3-D numerical simulations of thermocapillary flows in a shallow annular pool of silicon melt was conducted by means of the finite volume method. Simulations were conducted for a small annular melt pool ($r_o = 50$ mm and $r_i = 15$ mm) with a shallow depth $d = 3.0$ mm. From the simulation results, the following conclusions were obtained.

(1) The numerical results showed two possible types of 3-D oscillatory thermocapillary convections with different number of waves and different traveling directions in the annular pool of low-*Pr* silicon melt.
(2) The bifurcation is shown in the $V_{\theta,HW}$-*Ma* curve. The azimuthal velocity of the traveling hydrothermal wave and the number of spokes depend on *Ma*.
(3) With increasing *Ma*, the amplitude of the surface temperature fluctuation increases, but the frequency is less sensitive to *Ma*.

References

1. Smith, M.K., Davis, S.H.: Instabilities of dynamic thermocapillary liquid layers. Part 1. Convective instabilities. J. Fluid Mech. **132**, 119–144 (1993)
2. Garnier, N., Normand, C.: Effects of curvature on hydrothermal waves instability of radial thermocapillary flows. C. R. Acad. Paris, t. Series IV **2**, 1227–1233 (2001)
3. Villers, D., Platten, J.K.: Coupled buoyancy and Marangoni convection in acetone: experiments and comparison with numerical simulations. J. Fluid Mech. **234**, 487–510 (1992)
4. Daviaud, F., Vince, J.M.: Traveling waves in a fluid layer subjected to a horizontal temperature gradient. Phys. Rev. E **48**, 4432–4436 (1993)
5. Braunsfurth, M.G., Homsy, G.M.: Combined thermocapillary-buoyancy convection in a cavity. Part II. An Experimental Study. Phys. Fluids **9**, 1277–1286 (1997)
6. Garcimartin, A., Mukolobwiez, N., Daviaud, F.: Origin of waves in surface-tension-driven convection. Phys. Rev. E **56**, 1699–1705 (1997)
7. Riley, R.J., Neitzel, G.P.: Instability of thermocapillary–buoyancy convection in shallow layers. Part 1. Characterization of Steady and Oscillatory Instabilities. J. Fluid Mech. **359**, 143–164 (1998)
8. Benz, S., Hintz, P., Riley, R.J., Neitzel, G.P.: Instability of thermocapillary–buoyancy convection in shallow layers. Part Suppression of Hydrothermal Waves. J. Fluid Mech. **359**, 165–180 (1998)
9. Pelacho, M.A., Burguete, J.: Temperature oscillations of hydrothermal waves in thermocapillary–buoyancy convection. Phys. Rev. E **59**, 835–840 (1999)
10. Pelacho, M.A., Garcimartin, A., Burguete, J.: Marangoni number at the onset of hydrothermal waves. Phys. Rev. E **62**, 477–483 (2000)
11. Burguete, J., Mukolobwiez, N., Daviaud, F., Garnier, N., Chiffaudel, A.: Buoyant–thermocapillary instabilities in extended liquid layers subjected to a horizontal temperature gradient. Phys. Fluids **13**, 2773–2787 (2001)
12. Benz, S., Schwabe, D.: The three-dimensional stationary instability in dynamic thermocapillary shallow cavities. Exp. Fluids **31**, 409–416 (2001)
13. Ezersky, A.B., Garcimartin, A., Burguete, J., Mancini, H.L., Perez-Garcia, C.: Hydrothermal waves in Marangoni convection in a cylindrical container. Phys. Rev. E **47**, 1126–1131 (1993)
14. Mukolobwiez, N., Chiffaudel, A., Daviaud, F.: Supercritical Eckhaus instability for surface-tension-driven hydrothermal waves. Phys. Rev. Lett. **80**, 4661–4664 (1998)
15. Garnier, N., Chiffaudel, A.: Two dimensional hydrothermal waves in an extended cylindrical vessel. Eur. Phys. J. B **19**, 87–95 (2001)
16. Schwabe, D., Benz, S.: Thermocapillary flow instabilities in an annulus under microgravity –results of the experiment MAGIA. Adv. Space Res. **29**, 629–638 (2002)
17. Favre, E., Blumenfeld, L., Daviaud, F.: Instabilities of a liquid layer locally heated on its free surface. Phys. Fluids **9**, 1473–1475 (1997)
18. Schwabe, D., Zebib, A., Sim, B.C.: Oscillatory thermocapillary convection in open cylindrical annuli. Part 1 Experiments under Microgravity. J. Fluid Mech. **491**, 239–258 (2003)
19. Azami, T., Nakamura, S., Eguchi, M., Hibiya, T.: The role of surface-tension-driven flow in the formation of a surface pattern on a Czochralski silicon melt. J. Crystal Growth **233**, 99–107 (2001)
20. Ben Hadid, H., Roux, B.: Buoyancy and thermocapillary-driven flows in shallow open cavity unsteady flow regimes. J. Crystal Growth **97**, 217–225 (1989)
21. Ben Hadid, H., Roux, B.: Thermocapillary convection in long horizontal layers of low-Prandtl-number melts subject to a horizontal temperature gradient. J. Fluid Mech., **221**, 77–103 (1990)
22. Li, Y.R., Peng, L., Wu, S.Y., Zeng, D.L., Imaishi, N.: Thermocapillary convection in a differentially heated annular pool for moderate Prandtl number fluid. Int. J. Therm. Sci. **43**, 587–593 (2004)
23. Xu, J., Zebib, A.: Oscillatory two- and three-dimensional thermocapillary convection. J. Fluid Mech. **364**, 187–209 (1998)
24. Li, Y.R., Imaishi, N., Takeshi, T., Hibiya, T.: Three-dimensional oscillatory flow in a thin annular pool of silicon melt. J. Crystal Growth **260**, 28–42 (2004)
25. Li, Y.R., Peng, L., Akiyama, Y., Imaishi, N.: Three-dimensional numerical simulation of thermocapillary flow of moderate Prandtl number fluid in an annular pool. J. Crystal Growth **259**, 374–387 (2003)
26. Li, Y.R., Imaishi, N., Peng, L., Wu, S.Y., Hibiya, T.: Thermocapillary flow in shallow molten silicon pool with Czochralski configuration. J. Crystal Growth **266**, 88–95 (2004)
27. Li, Y.R., Ruan, D.F., Imaishi, N., Wu, S.Y., Peng, L., Zeng, D.L.: Global simulation of a silicon Czochralski furnace in an axial magnetic field. Int. J. Heat Mass Transf. **46**, 2887–2898 (2003)
28. Li, Y.R., Akiyama, Y., Imaishi, N., Tsukada, T.: Global analysis of a small Czochralski furnace with rotating crystal and crucible. J. Crystal Growth **255**, 81–92 (2003)
29. Patankar, S.V.: Numerical Heat Transfer and Fluid Flow. Hemisphere Publishing Co., New York (1980)